Title

Single-Molecule Detection of a Fluorescent Nucleobase Analogue via Multiphoton Excitation

Journal

The Journal of Physical Chemistry Letters, 10(17)

ISSN

1948-7185

Authors

Nobis, David
Fisher, Rachel S
Simmermacher, Mats
et al.

Publication Date

2019-09-05

DOI

10.1021/acs.jpclett.9b02108

Peer reviewed

HHS Public Access

Author manuscript

J Phys Chem Lett. Author manuscript; available in PMC 2020 September 05.

Published in final edited form as:

J Phys Chem Lett. 2019 September 05; 10(17): 5008–5012. doi:10.1021/acs.jpclett.9b02108.

Single-Molecule Detection of a Fluorescent Nucleobase Analogue via Multiphoton Excitation

David Nobis[†,‖], **Rachel S. Fisher**[‡,‖], **Mats Simmermacher**[‡], **Patrycja A. Hopkins**[§], **Yitzhak Tor**[§], **Anita C. Jones**[*,‡], **Steven W. Magennis**[*,†]

[†]WestCHEM School of Chemistry, University of Glasgow, Joseph Black Building, University Avenue, Glasgow G12 8QQ, U.K.

[‡]EaStCHEM School of Chemistry, The University of Edinburgh, Joseph Black Building, David Brewster Road, Edinburgh EH9 3FJ, U.K.

[§]Department of Chemistry and Biochemistry, University of California, San Diego, 9500 Gilman Drive, La Jolla, California 92093, United States

Abstract

The ability to routinely detect fluorescent nucleobase analogues at the single-molecule level would create a wealth of opportunities to study nucleic acids. We report the multiphoton-induced fluorescence and single-molecule detection of a dimethylamine-substituted extended-6-aza-uridine (**DMAthaU**). We show that **DMAthaU** can exist in a highly fluorescent form, emitting strongly in the visible region (470–560 nm). Using pulse-shaped broadband Ti:sapphire laser excitation, **DMAthaU** undergoes two-photon (2P) absorption at low excitation powers, switching to three-photon (3P) absorption at high incident intensity. The assignment of a 3P process is supported by cubic response calculations. Under both 2P and 3P excitation, the single-molecule brightness was over an order of magnitude higher than reported previously for any fluorescent base analogue, which facilitated the first single-molecule detection of an emissive nucleoside with multiphoton excitation.

Graphical Abstract

[*]**Corresponding Authors** a.c.jones@ed.ac.uk (A.C.J.)., steven.magennis@glasgow.ac.uk (S.W.M.).

[‖]These authors contributed equally.

The authors declare no competing financial interest.

ASSOCIATED CONTENT

Supporting Information

The Supporting Information is available free of charge on the ACS Publications website at DOI: 10.1021/acs.jp-clett.9b02108. Two-photon spectroscopy and cross section calculations, fluorescence lifetime measurements, calculation of dark-state population, multiphoton microscopy, computational methods, absorption, emission, and excitation spectra, fluorescence decays, plot of logarithmic dependence of the fluorescence intensity vs laser power, ratio of the SBR after shaping, rotamer structures, number of DNA molecules vs sample concentration, photon-counting histogram (Figures S1–S10); quantum yields and decay parameters (Tables S1–S4) (PDF)

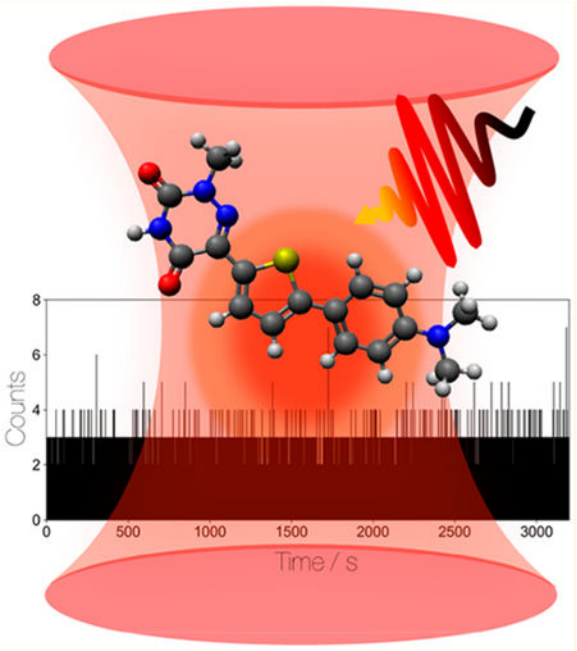

Fluorescence-based methods are powerful tools for studying the structure, dynamics, and interactions of nucleic acids *in vitro* and *in vivo,* and for technologies such as DNA sequencing and high-throughput screening. These methods typically involve covalent attachment of large fluorescent dyes via long linkers, but such labels are insensitive to local base interactions and may also perturb native interactions (e.g., with proteins).[1] Fluorescent base analogues (FBA) that preserve native nucleic acid structure can address such limitations,[2–10] but these have not yet found application in ultrasensitive analysis.[11–13] The main reasons for this are lower absorption cross section (ε) than for extrinsic dyes, limiting their brightness ($\varepsilon\Phi$, where Φ is the emission quantum yield), and short (UV) absorption wavelength, leading to photobleaching and poorer optical penetration into biological media.

A possible way to overcome these limitations is multiphoton excitation,[14–19] with potential benefits including deeper penetration into tissue in the near-IR, 3D control of excitation, and reduction of photobleaching and background fluorescence.[20,21] With the aim of reaching the ultimate single-molecule level of detection, we recently reported that an adenine analogue, pA, incorporated into single-stranded oligonucleotides could undergo two-photon (2P) excitation[22] and as few as five molecules could be detected.[23] Moreover, pA had enhanced photostability under 2P excitation. This demonstrated the feasibility of single-molecule detection, albeit improvements in brightness were still required.[23]

Here we demonstrate that an extended 6-aza-uridine ribonucleoside, **DMAthaU** (Chart 1), adopts a highly fluorescent form, in which the brightness following three-photon (3P) excitation is over an order of magnitude greater than that of pA under 2P excitation, allowing, for the first time, single-molecule detection via multiphoton excitation.

DMAthaU is a member of a family of tunable fluorescent 6-aza-uridines, the synthesis of which was reported previously.[24] Herein, we performed ensemble spectroscopic studies for

DMAthaU in either aqueous Tris buffer or dioxane. In buffer, the absorption maximum is at 385 nm while the excitation peak is blue-shifted to around 330 nm (Figure S1). The emission maximum is at 440 nm (Figure S2). The discrepancy between the excitation and absorption spectra indicates the presence of a dark (nonemissive) species, absorbing at longer wavelengths. This is confirmed by a strong dependence of the steady-state quantum yield (the average over all absorbing species) on the excitation wavelength (Table S1). The quantum yield (Φ) decreases from 0.05 to 0.003 on shifting the excitation wavelength from 330 to 380 nm. In dioxane, in contrast, the absorption and excitation spectra are identical (Figure S3) and coincide with the absorption spectrum in buffer. As reported previously,[24] the fluorescence of **DMAthaU** is responsive and dependent on solvent polarity; its emission spectrum in dioxane is red-shifted relative to that in buffer, and Φ is increased to 0.20.

Fluorescence decays of **DMAthaU** were recorded in buffer (Figure S4 and Tables S2 and S3) at three excitation wavelengths (364, 380, and 400 nm); these could be fitted globally to three decay components with common lifetimes of 0.19, 1.3, and 5.9 ns, respectively, but showed a marked dependence of A factors on excitation wavelength (Table S3). This results in a decrease in the average lifetime from 2.2 to 0.60 ns, on increasing the excitation wavelength from 360 to 400 nm. However, the decrease in average lifetime is not commensurate with the decrease in quantum yield, indicating the excitation of dark states at longer wavelengths. Further evidence of dark states comes from comparison of the average lifetimes and quantum yields in buffer and dioxane. In dioxane, an average lifetime of 1.8 ns (Table S4) corresponds to a quantum yield of 0.2, whereas in buffer, a $\langle \tau \rangle$ value of 2.2 ns (excitation at 380 nm) corresponds to a Φ of 0.003. On the basis of these values, assuming no dark states in dioxane, we estimate that 96% of the population excited at 380 nm in buffer is nonemissive (see the Supporting Information for details).

It is evident from the ensemble measurements that, in Tris buffer, **DMAthaU** exists in at least three emissive states and at least one dark state. This photophysical complexity is perhaps unsurprising given that **DMAthaU** can populate two distinct rotamers (with relative rotation of the azauridine and thiophene rings by 180°) and three tautomers, as illustrated in Chart 1. Ground-state density functional theory (DFT) calculations, in the gas phase and within a solvent continuum, show that the molecule exists preferentially as rotamer A (Chart 1), with rapid (nanoseconds) interconversion between rotamers.[25] In contrast, the three tautomers of the core 6-aza-uracil heterocycle have been shown to interconvert on much longer time scales (microseconds to milliseconds).[26] Although the ensemble-average quantum yield of **DMAthaU** in buffer is much less than that in dioxane, two of its emitting species have longer lifetimes, and hence higher individual quantum yields, than found in dioxane. We estimate that the longest lifetime species in buffer has an emission quantum yield of about 0.6.

Multiphoton excitation was first investigated in dioxane in ensemble measurements. The emission resulting from IR excitation (Figure S3) is attributed to a 2P process, based on the dependence of the emission intensity on laser power (Figure S5); the log–log plot following excitation at 840 nm has a slope of 1.85 ± 0.04. Since 2P excitation results in the same emission spectrum as that seen for one-photon (1P) excitation (Figure S3), the emission is dominated by the same species in each instance. The 2P cross-section of **DMAthaU** in

dioxane, measured relative to rhodamine 6G, is 90.0 ± 5.0 GM with a corresponding 2P brightness of 18 GM. This cross-section is higher than that of any other FBA studied previously, including pA (21 GM in ethanol[23]), and the brightness is 3 times greater than that of pA.

Given the existence of **DMAthaU** in a highly fluorescent state (albeit with a low population), we were encouraged to pursue single-molecule detection in buffer. The multiphoton excitation of **DMAthaU** in buffer was investigated using a home-built microscope with broadband femtosecond laser excitation and photon-counting detection.[23] Measurement and compensation for dispersion in the optical system[27] is achieved by dual amplitude and phase-shaping of the laser pulse, using multiphoton intrapulse interference phase scan (MIIPS).[28] The spectral width and center of the laser spectrum were varied to optimize the signal-to-background ratio (SBR, Figure S6). This improved the SBR by a factor of 1.6 (Figure 1).

The power dependence for a solution of **DMAthaU** in buffer (Figure 2) is rather different from that measured in dioxane (Figure S5). At low powers, the curve has a slope of ~2, which switches at higher powers to a slope of ~3, indicative of 3P absorption. At the highest laser powers, saturation occurs. As discussed above, the 1P excitation maximum is blue-shifted with respect to the absorption peak (Figure S1), so the excitation maximum at twice the 1P wavelength has a weak overlap with the laser spectrum (Figure 1). In contrast, tripling the 1P excitation wavelength gives a very good match to the laser spectrum, particularly with the optimized pulse (Figure 1). The decay parameters measured in either the 2P or 3P excitation regimes are essentially identical (considering the excitation-wavelength dependence) to those for 1P excitation, confirming that the emission originates from the same excited states in each case (Figure S7).

In support of the assignment of 3P excitation, we performed cubic response calculations within time-dependent density functional theory (TDDFT) for the two optimized rotamer structures (Figure S8). The key finding (Table 1) is that for both rotamers there are particularly strong 3P transitions (the fifth and sixth) that display degenerate 3P absorption wavelengths close to the maximum of the optimized laser spectrum (Figure 1). Furthermore, the magnitude of the calculated 3P cross sections are in agreement with estimated 3P cross sections[29] and those measured for fluorophores of similar size.[30]

Next, we examined the limits of detection of **DMAthaU** in buffer, using fluorescence correlation spectroscopy (FCS) and photon-counting with a multichannel scaler (MCS), similar to our recent work with pA.[23] Excitation powers of 10 mW, where the 3P excitation begins to saturate, gave the best SBR; the pulses were compressed to 8 fs at the focal plane before additional shaping was applied.

In FCS measurements there was a striking discrepancy between the known sample concentration and the number of molecules observed in the laser focus. The correlation curve in Figure 3 was recorded for a 525 nM solution, as determined by UV-vis absorption.[24] On average ~0.4 molecule was found in the focus at this concentration. In contrast, for Rh110 at 10 nM there were ~1.4 molecules in the focus. Assuming all of the Rh110

molecules are detected, this implies that ~1/180 of the **DMAthaU** molecules that go through the focus are emissive, which agrees with the finding from bulk measurements that ~96% of the molecules are in a dark state. On the basis of the discussion above, and previous reports of tautomerism of FBAs,[40–42] we assign this dark state to a long-lived tautomer of **DMAthaU**.[26]

The diffusion time of **DMAthaU** is 25 μs, which is commensurate with the size of the freely diffusing ribonucleoside and is independent of the sample concentration. The number of detected molecules scales linearly with concentration (Figure S9). For those **DMAthaU** molecules in the bright state, the single-molecule brightness, as given by the count rate per molecule (CPM), is 6.9 ± 0.2 kHz/molecule, over an order of magnitude higher than for pA.[23]

The high brightness of **DMAthaU** determined by FCS motivated us to attempt single-molecule detection. An MCS trace was recorded for a dilute solution (~10^{-11} M of bright **DMAthaU** molecules) (Figure 4a) and compared to a measurement of pure buffer (Figure 4b). Single molecules of **DMAthaU** are clearly identified as short-lived (ms) bursts on the background (see Figure S10 for a detailed burst analysis). Although the bursts are small, their magnitude agrees with the CPM derived from FCS (note that the CPM for the sample in Figure 4 is closer to 5 kHz/molecule due to the presence of additional filters to further optimize the SBR).

In conclusion, we have shown for the first time that an FBA, an extended 6-aza-uridine ribonucleoside (**DMAthaU**), can be detected at the single-molecule level using multiphoton excitation. This highly fluorescent species is a monomer of **DMAthaU**, which undergoes 3P excitation at ~800 nm, as supported by TDDFT calculations. Future studies will focus on incorporating **DMAthaU** into DNA and RNA. It will be particularly interesting to see which species are present in DNA/RNA and how the presence of neighboring bases influences the brightness of **DMAthaU**. In this context, the quantum yield in dioxane suggests that we may have additional enhancements in brightness due to changes in the local environment upon incorporation in an oligonucleotide. The potential for unprecedented insight into the mechanism of processes involving nucleic acids at the individual base level may soon be realized.

Supplementary Material

Refer to Web version on PubMed Central for supplementary material.

ACKNOWLEDGMENTS

This work was supported by EPSRC (studentships for DN and RSF) and the University of Edinburgh (RSF). We thank the National Institutes of Health for generous support (via grant number GM 069773).

Research data supporting this publication can be found at http://dx.doi.org/10.5525/gla.researchdata.837.

REFERENCES

(1). Stennett EMS; Ciuba MA; Lin S; Levitus M Demystifying PIFE: The Photophysics Behind the Protein-Induced Fluorescence Enhancement Phenomenon in Cy3. J. Phys. Chem. Lett 6, 1819–1823.

(2). Wilhelmsson LM Fluorescent Nucleic Acid Base Analogues. Q. Rev. Biophys 2010, 43, 159–183. [PubMed: 20478079]

(3). Sinkeldam RW; Greco NJ; Tor Y Fluorescent Analogs of Biomolecular Building Blocks: Design, Properties, and Applications. Chem. Rev 2010, 110, 2579–2619. [PubMed: 20205430]

(4). Xu W; Chan KM; Kool ET Fluorescent Nucleobases as Tools for Studying DNA and RNA. Nat. Chem 2017, 9, 1043–1055. [PubMed: 29064490]

(5). Burns DD; Teppang KL; Lee RW; Lokensgard ME; Purse BW Fluorescence Turn-On Sensing of DNA Duplex Formation by a Tricyclic Cytidine Analogue. J. Am. Chem. Soc 2017, 139, 1372–1375. [PubMed: 28080035]

(6). Shin D; Sinkeldam RW; Tor Y Emissive RNA Alphabet. J. Am. Chem. Soc 2011, 133, 14912–14915.

(7). Rovira AR; Fin A; Tor Y Chemical Mutagenesis of an Emissive RNA Alphabet. J. Am. Chem. Soc 2015, 137, 14602—14605.

(8). Wranne MS; Fuchtbauer AF; Dumat B; Bood M; El-Sagheer AH; Brown T; Graden H; Grotli M; Wilhelmsson LM Toward Complete Sequence Flexibility of Nucleic Acid Base Analogue FRET. J. Am. Chem. Soc 2017, 139, 9271–9280. [PubMed: 28613885]

(9). Han JH; Yamamoto S; Park S; Sugiyama H Development of a Vivid FRET System Based on a Highly Emissive dG-dC Analogue Pair. Chem. - Eur. J 2017, 23, 7607–7613. [PubMed: 28411372]

(10). Jones AC; Neely RK 2-Aminopurine as a Fluorescent Probe of DNA Conformation and the DNA-Enzyme Interface. Q Rev. Biophys 2015, 48, 244–279. [PubMed: 25881643]

(11). Wennmalm S; Blom H; Wallerman L; Rigler R UV-Fluorescence Correlation Spectroscopy of 2-Aminopurine. Biol. Chem 2001, 382, 393–397. [PubMed: 11347886]

(12). Sanabia JE; Goldner LS; Lacaze PA; Hawkins ME On the Feasibility of Single-Molecule Detection of the Guanosine-Analogue 3-MI. J. Phys. Chem. B 2004, 108, 15293–15300.

(13). Aleman EA; de Silva C; Patrick EM; Musier-Forsyth K; Rueda D Single-Molecule Fluorescence Using Nucleotide Analogs: A Proof-of-Principle. J. Phys. Chem. Lett 2014, 5, 777–781. [PubMed: 24803990]

(14). Katilius E; Woodbury NW Multiphoton Excitation of Fluorescent DNA Base Analogs. J. Biomed. Opt 2006, 11, 044004.

(15). Stanley RJ; Hou ZJ; Yang AP; Hawkins ME The Two-Photon Excitation Coss Section of 6MAP, a Fluorescent Adenine Analogue. J. Phys. Chem. B 2005, 109, 3690–3695. [PubMed: 16851408]

(16). Lane RSK; Magennis SW Two-Photon Excitation of the Fluorescent Nucleobase Analogues 2-AP and tC. RSC Adv. 2012, 2, 11397—11403.

(17). Mikhaylov A; de Reguardati S; Pahapill J; Callis PR; Kohler B; Rebane A Two-Photon Absorption Spectra of Fluorescent Isomorphic DNA Base Analogs. Biomed. Opt. Express 2018, 9, 447–452. [PubMed: 29552385]

(18). Lane RSK; Jones R; Sinkeldam RW; Tor Y; Magennis SW Two-Photon-Induced Fluorescence of Isomorphic Nucleobase Analogs. ChemPhysChem 2014, 15, 867–871. [PubMed: 24604669]

(19). Stoltzfus CR; Rebane A Optimizing Ultrafast Illumination for Multiphoton-Excited Fluorescence Imaging. Biomed. Opt. Express 2016, 7, 1768–1782. [PubMed: 27231620]

(20). He GS; Tan LS; Zheng Q; Prasad PN Multiphoton Absorbing Materials: Molecular Designs, Characterizations, and Applications. Chem. Rev 2008, 108, 1245–1330. [PubMed: 18361528]

(21). Zipfel WR; Williams RM; Webb WW Nonlinear Magic: Multiphoton Microscopy in the Biosciences. Nat. Biotechnol 2003, 21, 1369–1377. [PubMed: 14595365]

(22). Bood M; Fuchtbauer AF; Wranne MS; Ro JJ; Sarangamath S; El-Sagheer AH; Rupert DLM; Fisher RS; Magennis SW; Jones AC; Hook F; Brown T; Kim BH; Dahlen A; Wilhelmsson LM;

Grotli M Pentacyclic Adenine: a Versatile and Exceptionally Bright Fluorescent DNA Base Analogue. Chem. Sci 2018, 9, 3494–3502. [PubMed: 29780479]

(23). Fisher RS; Nobis D; Fuchtbauer AF; Bood M; Grotli M; Wilhelmsson LM; Jones AC; Magennis SW Pulse-Shaped Two-Photon Excitation of a Fluorescent Base Analogue Approaches Single-Molecule Sensitivity. Phys. Chem. Chem. Phys 2018, 20, 28487–28498.

(24). Hopkins PA; Sinkeldam RW; Tor Y Visibly Emissive and Responsive Extended 6-Aza-Uridines. Org. Lett 2014, 16, 5290–5293. [PubMed: 25285451]

(25). Fisher RS Photophysical Characterisation of Fluorescent Base Analogues. Ph.D Thesis. The University of Edinburgh, 2018.

(26). Markova N; Pejov L; Enchev V A Hybrid Statistical Mechanics-Quantum Chemical Model for Proton Transfer in 5-Azauracil and 6-Azauracil in Water Solution. Int. J. Quantum Chem 2015, 115, 477–485.

(27). Pastirk I; Dela Cruz JM; Walowicz KA; Lozovoy VV; Dantus M Selective Two-Photon Microscopy with Shaped Femto-second Pulses. Opt. Express 2003, 11, 1695–1701. [PubMed: 19466048]

(28). Lozovoy VV; Pastirk I; Dantus M Multiphoton Intrapulse Interference. IV. Ultrashort Laser Pulse Spectral Phase Characterization and Compensation. Opt. Lett 2004, 29, 775–777. [PubMed: 15072388]

(29). Xu C; Webb WW Multiphoton Excitation of Molecular Fluorophores and Nonlinear Laser Microscopy; Plenum Press: New York, 1997; Vol. 5, pp 471–540.

(30). Shear JB; Brown EB; Webb WW Multiphoton-Excited Fluorescence of Fluorogen-Labeled Neurotransmitters. Anal. Chem 1996, 68, 1778–1783. [PubMed: 8651483]

(31). Jansik B; Salek P; Jonsson D; Vahtras O; Agren H Cubic Response Functions in Time-Dependent Density Functional Theory. J. Chem. Phys 2005, 122, 054107.

(32). Yanai T; Tew DP; Handy NC A New Hybrid Exchange-Correlation Functional using the Coulomb-Attenuating Method (CAM-B3LYP). Chem. Phys. Left 2004, 393, 51–57.

(33). Dunning TH Gaussian-Basis Sets For Use In Correlated Molecular Calculations. 1. The Atoms Boron Through Neon Ans Hydrogen. J. Chem. Phys 1989, 90, 1007–1023.

(34). Woon DE; Dunning TH Gaussian-Basis Sets For Use In Correlated Molecular Calculations. 3. The Atoms Aluminum Through Argon. J. Chem. Phys 1993, 98, 1358–1371.

(35). Aidas K; et al. The Dalton Quantum Chemistry Program System. WIREs-Comput. Mol. Sci 2014, 4, 269–284.

(36). Dalton, a Molecular Electronic Structure Program, Release v2019.alpha; 2018; see http://daltonprogram.org/.

(37). Becke AD Density-Functional Thermochemistry 0.3. The Role of Exact Exchange. J. Chem. Phys 1993, 98, 5648–5652.

(38). Cronstrand P; Jansik B; Jonsson D; Luo Y; Agren H Density Functional Response Theory Calculations of Three-Photon Absorption. J. Chem. Phys 2004, 121, 9239–9246. [PubMed: 15538844]

(39). Friese DH; Beerepoot MTP; Ringholm M; Ruud K Open-Ended Recursive Approach for the Calculation of Multiphoton Absorption Matrix Elements. J. Chem. Theory Comput 2015, 11, 1129–1144. [PubMed: 25821415]

(40). Neely RK; Magennis SW; Dryden DTF; Jones AC Evidence of Tautomerism in 2-Aminopurine from Fluorescence Lifetime Measurements. J. Phys. Chem. B 2004, 108, 17606–17610.

(41). Stengel G; Purse BW; Wilhelmsson LM; Urban M; Kuchta RD Ambivalent Incorporation of the Fluorescent Cytosine Analogues tC and tCo by Human DNA Polymerase alpha and Klenow Fragment. Biochemistry 2009, 48, 7547–7555. [PubMed: 19580325]

(42). Sholokh M; Improta R; Mori M; Sharma R; Kenfack C; Shin D; Voltz K; Stote RH; Zaporozhets OA; Botta M; Tor Y; Mely Y Tautomers of a Fluorescent G Surrogate and Their Distinct Photophysics Provide Additional Information Channels. Angew. Chem., Int. Ed 2016, 55, 7974–7978.

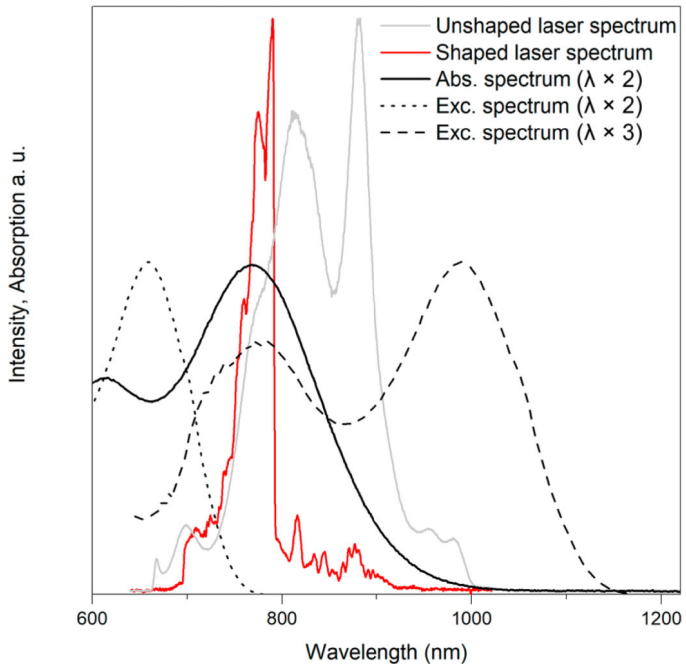

Figure 1.

Laser excitation profiles, unshaped (gray line) and pulse-shaped (red line), compared with the **DMAthaU** one-photon absorption spectrum (black line, plotted against double the one-photon wavelength) and the one-photon excitation spectrum plotted against double (dotted line) and triple (dashed line) the one-photon wavelength.

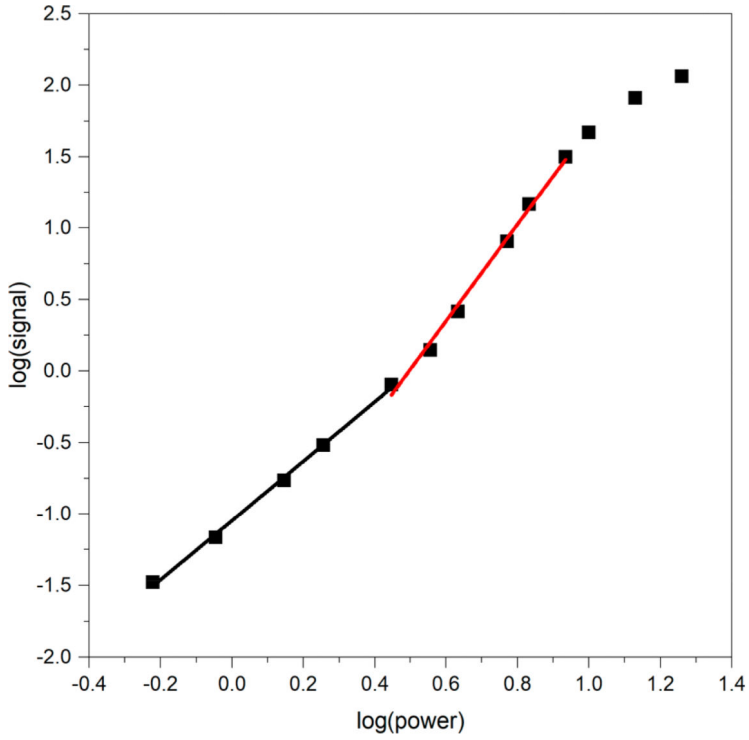

Figure 2.

Power-dependence of **DMAthaU** emission intensity in buffer. The lower part of the curve (pulse energy <35 pJ) was fitted with a slope of 2.1 (black line). At higher powers (pulse energy 35–107 pJ), the slope is 3.3 (red line).

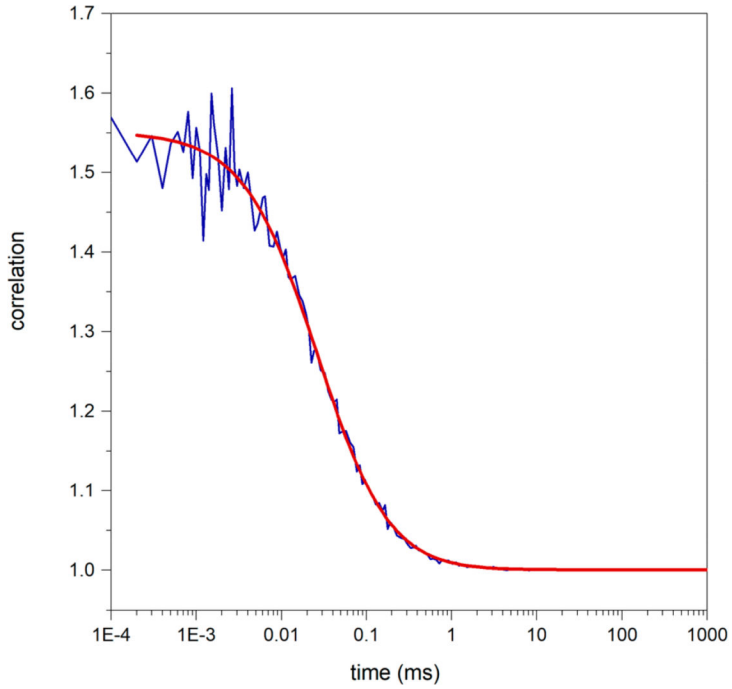

Figure 3.

FCS curve of **DMAthaU** in buffer at pH 7.7. The blue line depicts the data, and the fit is shown in red for a single emitting species undergoing diffusion in a 3D Gaussian volume. The average number of molecules in the focus is 0.5.

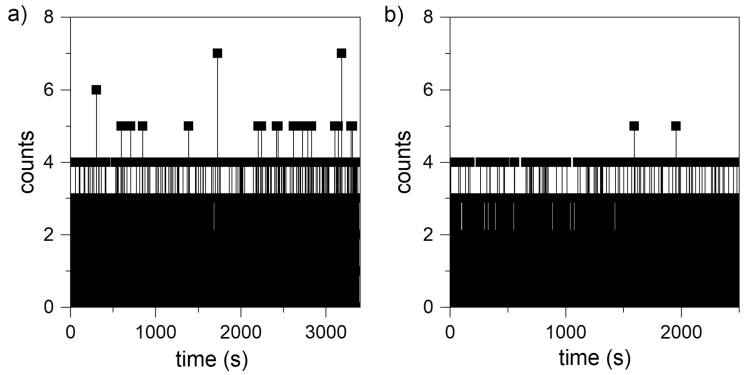

Figure 4.

Single-molecule traces with laser power corresponding to the 3P regime for (a) **DMAthaU** diluted in buffer (1×10^{-11} M of bright molecules) and (b) buffer only.

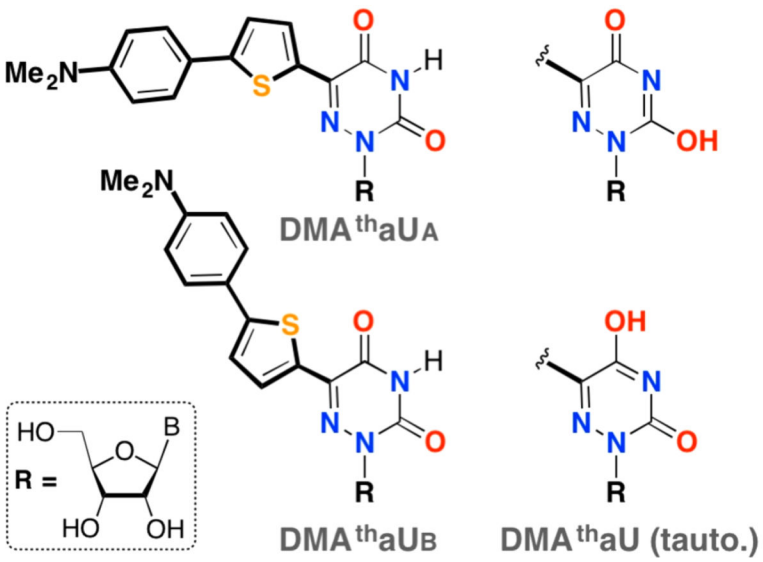

Chart 1.
Rotameric and Tautomeric Structures of the Extended Thiophene-6-aza-uridine, DMAthaU

Table 1.

Degenerate Three-Photon Absorption Wavelengths λ^{3PA}(nm) and Three-Photon Absorption Cross Sections σ^{3PA} (10^{-82} cm^6 s^2 $photon^{-2}$) for the First Ten Transitions from the Electronic Ground States of Two Rotamers $DMA^{th}aU\_A$ and $DMA^{th}aU\_B$[a]

	$DMA^{th}aU\_A$		$DMA^{th}aU\_B$	
	λ^{3PA}	σ^{3PA}	λ^{3PA}	σ^{3PA}
1	1110	59.9	1120	67.4
2	834	100	838	22.4
3	825	0.457	827	18.0
4	818	7.90	816	38.4
5	790	1,940	785	10,800
6	769	12,500	777	3,590
7	695	5.98	698	6.94
8	680	48.0	683	64.5
9	655	65.8	657	97.0
10	648	13.9	647	7.26

[a]The values are calculated with CAM-B3LYP/cc-pVDZ for linearly polarized light and nuclear geometries optimized with B3LYP/cc-pVTZ (see the Supporting Information and refs 31–39).